Nanofocusing in laterally tapered plasmonic waveguides

Ewold Verhagen, Albert Polman, and L. (Kobus) Kuipers

Center for Nanophotonics, FOM-Institute for Atomic and Molecular Physics (AMOLF), Kruislaan 407, 1098 SJ Amsterdam, The Netherlands
verhagen@amolf.nl

Abstract: We investigate the focusing of surface plasmon polaritons (SPPs) excited with 1.5 μm light in a tapered Au waveguide on a planar dielectric substrate by experiments and simulations. We find that nanofocusing can be obtained when the asymmetric bound mode at the substrate side of the metal film is excited. The propagation and concentration of this mode to the tip is demonstrated. No sign of a cutoff waveguide width is observed as the SPPs propagate along the tapered waveguide. Simulations show that such concentrating behavior is not possible for excitation of the mode at the low-index side of the film. The mode that enables the focusing exhibits a strong resemblance to the asymmetric mode responsible for focusing in conical waveguides. This work demonstrates a practical implementation of plasmonic nanofocusing on a planar substrate.

OCIS codes: (240.6680) Optics at surfaces; (250.5403) Optoelectronics; (050.6624) Diffraction and gratings; (310.2790) Thin films.

References and links

1. E. Ozbay, "Plasmonics: Merging photonics and electronics at nanoscale dimensions," Science **311**, 189-193 (2006).
2. J.-C. Weeber, J. R. Krenn, A. Dereux, B. Lamprecht, Y. Lacroute, J. P. Goudonnet, "Near-field observation of surface plasmon polariton propagation on thin metal stripes," Phys. Rev. B **61**, 045411 (2001).
3. A. Hohenau, J. R. Krenn, A. L. Stepanov, A. Drezet, H. Ditlbacher, B. Steinberger, A. Leitner, F. R. Aussenegg, "Dielectric optical elements for surface plasmons," Opt. Lett. **30**, 893-895 (2005).
4. A. Drezet, A. L. Stepanov, H. Ditlbacher, B. Steinberger, F. R. Aussenegg, A. Leitner, J. R. Krenn, "Surface plasmon propagation in an elliptical corral," Appl. Phys. Lett. **86**, 074104 (2005).
5. L. Yin, V. K. Vlasko-Vlasov, J. Pearson, J. M. Hiller, J. Hua, U. Welp, D. E. Brown, C. W. Kimball, "Subwavelength focusing and guiding of surface plasmons," Nano Lett. **5**, 1399-1402 (2005).
6. Z. Liu, J. M. Steele, W. Srituravanich, Y. Pikus, C. Sun, X. Zhang, "Focusing surface plasmons with a plasmonics lens," Nano Lett. **5**, 1726-1729 (2005).
7. H. L. Offerhaus, B. van den Bergen, M. Escalante, F. B. Segerink, J. P. Korterik, N. F. van Hulst, "Creating focused plasmons by noncollinear phasematching on functional gratings," Nano Lett. **5**, 2144-2148 (2005).
8. C. A. Pfeiffer, E. N. Economou, K. L. Ngai, "Surface polaritons in a circularly cylindrical interface: surface plasmons," Phys. Rev. B **10**, 3038-3051 (1974).
9. J. J. Burke and G. I. Stegeman, "Surface-polariton-like waves guided by thin, lossy metal films," Phys. Rev. B **33**, 5186-5201 (1986).
10. E. N. Economou, "Surface plasmons in thin films," Phys. Rev. **182**, 539-554 (1969).
11. M. I. Stockman, "Nanofocusing of optical energy in tapered plasmonic waveguides," Phys. Rev. Lett. **93**, 137404 (2004).
12. D. K. Gramotnev and K. C. Vernon, "Adiabatic nano-focusing of plasmons by sharp metallic wedges," Appl. Phys. B **86**, 7-17 (2007).
13. D. K. Gramotnev, D. F. P. Pile, M. W. Vogel, X. Zhang, "Local electric field enhancement during nanofocusing of plasmons by a tapered gap," Phys. Rev. B **75**, 035431 (2007).
14. F. Keilmann, "Surface-polariton propagation for scanning near-field optical microscopy application," J. Microsc. **194**, 567-570 (1999).
15. A. Bouhelier, J. Renger, M. R. Beversluis, L. Novotny, "Plasmon-coupled tip-enhanced near-field optical microscopy," J. Microsc. **210**, 220-224 (2003).
16. C. Ropers, C. C. Neacsu, T. Elsaesser, M. Albrecht, M. B. Raschke, C. Lienau, "Grating-coupling of surface plasmons onto metallic tips: A nanoconfined light source," Nano Lett. **7**, 2784-2788 (2007).

#89786 - $15.00 USD Received 14 Nov 2007; revised 19 Dec 2007; accepted 19 Dec 2007; published 2 Jan 2008

17. J. Koglin, U. C. Fischer, H. Fuchs, "Material contrast in scanning near-field optical microscopy at 1-10 nm resolution," Phys. Rev. B **55**, 7977-7984 (1997).
18. N. A. Janunts, K. S. Baghdasaryan, Kh. V. Nerkararyan, B. Hecht, "Excitation and superfocusing of surface plasmon polaritons on a silver-coated optical fiber tip," Opt. Commun. **253**, 118-124 (2005).
19. E. Verhagen, L. Kuipers, A. Polman, "Enhanced nonlinear optical effects with a tapered plasmonic waveguide," Nano Lett. **7**, 334-337 (2007).
20. E. Verhagen, A. L. Tchebotareva, A. Polman, "Erbium luminescence imaging of infrared surface plasmon polaritons," Appl. Phys. Lett. **88**, 121121 (2006).
21. R. Zia, J. A. Schuller, M. L. Brongersma, "Near-field characterization of guided polariton propagation and cutoff in surface plasmon waveguides," Phys. Rev. B **74**, 165415 (2006).
22. D. S. Kim, S. C. Hohng, V. Malyarchuk, Y. C. Yoon, Y. H. Ahn, K. J. Yee, J. W. Park, J. Kim, Q. H. Park, C. Lienau, "Microscopic origin of surface-plasmon radiation in plasmonic band-gap nanostructures," Phys. Rev. Lett. **91**, 143901 (2003).
23. E. Devaux, T. W. Ebbesen, J.-C. Weeber, A. Dereux, "Launching and decoupling surface plasmons via micro-gratings," Appl. Phys. Lett. **83**, 4936-4938 (2003).
24. F. Auzel, "Upconversion and anti-Stokes processes with f and d ions in solids," Chem. Rev. **104**, 139-173 (2004).
25. G. N. van den Hoven, E. Snoeks, A. Polman, C. van Dam, J. W. M. van Uffelen, M. K. Smit, "Upconversion in Er-implanted Al_2O_3 waveguides," J. Appl. Phys. **79**, 1258-1266 (1996).
26. G. N. van den Hoven, E. Snoeks, A. Polman, J. W. M. van Uffelen, Y. S. Oei, M. K. Smit, "Photoluminescence characterization of Er-implanted Al_2O_3 films," Appl. Phys. Lett. **62**, 3065-3067 (1993).
27. M. Pollnau, D. R. Gamelin, S. R. Lüthi, H. U. Güdel, M. P. Hehlen, "Power dependence of upconversion luminescence in lanthanide and transition-metal-ion systems," Phys. Rev. B **61**, 3337-3346 (2000).
28. R. Zia, M. D. Selker, M. L. Brongersma, "Leaky and bound modes of surface plasmon waveguides," Phys. Rev. B **71**, 165431 (2005).
29. *Lumerical FDTD Solutions 5.0*
30. P. Berini, "Plasmon-polariton waves guided by thin lossy metal films of finite width: Bound modes of asymmetric structures," Phys. Rev. B **63**, 125417 (2001).
31. P. B. Johnson and R. W. Christy, "Optical constants of the noble metals," Phys. Rev. B **6**, 4370-4379 (1972)
32. Z. Zhu and T. G. Brown, "Full-vectorial finite-difference analysis of microstructured optical fibers," Opt. Express **10**, 853-864 (2002).
33. H. Ditlbacher, A. Hohenau, D. Wagner, U. Kreibig, M. Rogers, F. Hofer, F. R. Aussenegg, J. R. Krenn, "Silver nanowires as surface plasmon resonators," Phys. Rev. Lett. **95**, 257403 (2005).

1. Introduction

The ability of properly shaped metal nanostructures to tightly confine optical energy lies at the heart of the current interest in plasmonics [1]. Large field enhancements in small volumes offer benefits in sensing, control of optical signals, data storage, nanolithography and addressing single quantum emitters. The efficient delivery of light at these small scales is therefore an issue of crucial importance. Because surface plasmon polariton (SPP) waves supported by metal/dielectric interfaces can exhibit in-plane wave vectors larger than that of light with the same frequency, SPPs are suitable to achieve focusing to length scales smaller than the diffraction limit of light in the surrounding dielectric. A variety of focusing geometries has been used to demonstrate the concentration of SPPs supported by planar metal/dielectric interfaces [2-7]. Achieving focusing of SPPs to truly nanoscale dimensions will, for most frequencies, require wave vectors that are much larger than those for SPPs on an extended flat metal/dielectric interface. Complex waveguiding geometries that do exhibit larger wave vectors are for example: the azimuthally symmetric mode supported by a narrow metal cylinder [8], the mode in a thin metal slab embedded between two dielectrics that has an asymmetric transverse electric field across the film [9], or the mode propagating in a thin dielectric slab between two metal half-spaces [10]. By gradually reducing the thickness of these geometries along the direction of propagation, the SPP modes they support are predicted to become more strongly confined and concentrated to very small dimensions [11-13]. Demonstrating this effect requires the challenging fabrication of very sharp conical metal tips [14-18], metallic wedges, or nanoscale gaps. Moreover, the requirement of asymmetric

#89786 - $15.00 USD Received 14 Nov 2007; revised 19 Dec 2007; accepted 19 Dec 2007; published 2 Jan 2008

transverse modal fields in the first two geometries makes excitation of the required SPP modes not straightforward.

Here, we present the possibility to achieve nanofocusing of SPPs with a laterally tapered metal stripe waveguide on a dielectric substrate, both in experiment and simulations. The purely bound SPP mode at the high-index side of the tapered waveguide is excited with light of a wavelength of 1.48 μm in air. In this respect, the experiment differs significantly from that by Weeber et al. [2], who excite SPPs at the air side of a similar structure. As we will show in this paper this is an essential difference with regard to whether nanofocusing can be achieved efficiently. We observe the focusing of SPPs in the tapered waveguide by detecting upconversion luminescence from erbium ions implanted in the substrate [19,20]. A detailed study of the upconversion luminescence intensity distribution shows that SPPs are guided and concentrated along the taper all the way to its tip. No sign of a cutoff width is observed for the mode excited at the metal/substrate interface. These results suggest the excitation of a SPP mode that remains closely bound to the metal and has an increasing wave vector along the taper. It allows the desired focusing at the taper tip.

To explain the experimental findings we perform finite-difference time-domain (FDTD) calculations of the electromagnetic field in this structure. We find that strong field confinement and concentration at the taper tip is indeed possible when the purely bound SPP mode propagating at the substrate side of the metal film is excited. This focusing is absent for the leaky SPP mode that propagates predominantly at the air side of the metal, which is the mode that is usually studied in near-field experiments [2,5,21]. Based on the FDTD simulations we explain the different behavior of these modes by symmetry arguments. These results provide insight in the mechanism of guiding and nanofocusing in complex SPP tapering geometries and show how such nanofocusing can be achieved using a structured metal film on a planar substrate.

2. Sample fabrication and experimental technique

Because we are interested in the behavior of purely bound SPP modes propagating at the substrate side of a metal film on a dielectric substrate, Kretschmann-Raether coupling cannot be used to excite the SPPs. Instead, a subwavelength hole array is illuminated to achieve the necessary momentum matching of an incident 1.48 μm light beam to SPPs. Such a geometry has been used before to excite SPPs at the air side of a metal film [22,23]. The excited SPPs are subsequently coupled into a laterally tapered waveguide structured in the Au film. To image the SPP field, which is predominantly localized at the substrate side of the metal, erbium ions implanted just beneath the surface of the sapphire substrate are used as a probe of the SPP near field [19,20]. Because energy levels of Er^{3+} that emit visible light can be populated under 1.48 μm excitation through a nonlinear upconversion process, the infrared SPP field can be imaged using visible wavelengths. Figure 1(a) shows the Er^{3+} energy level diagram, in which the cooperative upconversion process is depicted that is the dominant mechanism exciting higher energy levels with 1.48 μm pump light [24,25]. In this nonlinear process, two Er ions that are both excited to the first excited state can exchange energy through Förster transfer, thereby demoting one ion to the ground state and promoting the other to the $^4I_{9/2}$ level. The latter ion quickly relaxes to the $^4I_{11/2}$ state, from where it can decay nonradiatively or through the emission of a 980 nm photon. It can also interact with one or two excited Er ions again to populate the $^4F_{9/2}$ and $^4S_{3/2}$ manifolds, which emit photons at 660 and 550 nm, respectively. The emission of these two levels is used here to probe the infrared SPP pump field.

#89786 - $15.00 USD Received 14 Nov 2007; revised 19 Dec 2007; accepted 19 Dec 2007; published 2 Jan 2008

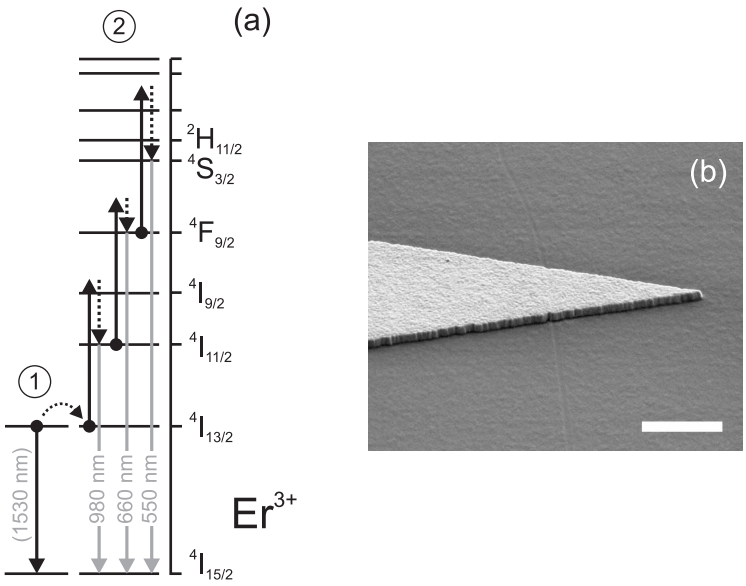

Fig. 1. (a) Energy level diagram of Er^{3+} ions. The black arrows depict the cooperative upconversion mechanism which causes the excitation of higher energy levels by energy transfer between two excited ions. (b) SEM image of the end of a fabricated, tapered Au waveguide on an Er-implanted sapphire substrate. The scale bar is 1 µm.

A 400 µm thick sapphire substrate (refractive index 1.74) is implanted with 200 keV Er^+ ions at a fluence of 7×10^{15} cm^{-2} through a 10 nm thick Ge conducting layer, which is subsequently removed. This results in a Gaussian Er depth distribution centered 35 nm below the sapphire surface with a standard deviation of σ = 12 nm, as simulated with the Monte Carlo program SRIM. The sample is annealed under an Ar atmosphere at 900 °C for one hour to remove implantation related defects and activate the Er ions [26].

To fabricate the patterned Au film, the substrate is first coated with a layered stack consisting of 300 nm photoresist (S1813), 20 nm Ge and 110 nm negative electron beam resist (Ma-N 2401). Taper and hole array structures are patterned in the electron beam resist layer with electron beam lithography, and this pattern is transferred to the layers underneath by reactive ion etching. A 100 nm thick Au film is then evaporated directly on the substrate through resistive heating. Finally, the remaining photoresist is stripped in a liftoff process. A SEM micrograph of the tip of a typical taper fabricated this way is shown in Fig. 1(b). The apex diameter of the taper tip is found to be 65±5 nm.

A fiber-pigtailed 1.48 µm diode pump laser (Fitel) is used as excitation source. Figure 2 shows a schematic of the hole array/taper geometry. The pitch of the hole array is chosen such that p-polarized light with a wavelength of 1.48 µm is diffracted to generate SPPs propagating at the substrate side of the film. To maximize the excitation of the desired SPP mode, the excitation beam is focused to a 10 µm wide spot near the edge of the array. The triangularly shaped tapered waveguide starts at a distance of 6 µm from the edge of the excitation array and has a base width of 12 µm and a length of 60 µm (taper angle 11.4°).

Two-dimensional maps of the SPP field intensity under the taper are obtained by detecting the luminescence of the Er ions implanted close to the Au/substrate interface in a scanning confocal microscope. The experiment is performed in two configurations. In the geometry of Fig. 2(a), the sample is illuminated from the air side of the film under normal incidence through a microscope objective (NA = 0.12). In order to excite SPPs on the substrate side of the film, the pitch of the hole array is 0.8 µm. The upconversion luminescence is collected through the substrate by a 50× microscope objective (Nikon L Plan EPI CR, NA = 0.7). A rotated identical sapphire substrate is used below the implanted one to

#89786 - $15.00 USD Received 14 Nov 2007; revised 19 Dec 2007; accepted 19 Dec 2007; published 2 Jan 2008

correct for the birefringence of sapphire, and the microscope objective is corrected to reduce the effect of spherical aberration induced by imaging through the two substrates. In the configuration of Fig. 2(b), the sample is illuminated through the substrate under an angle of 47° with respect to the surface normal using a fiber focuser (NA = 0.1). Also in this configuration SPPs are excited on the substrate side of the film through the hole array that has a pitch of 1.46 µm. A 100× objective (Zeiss Epiplan-Neofluar, NA = 0.9) is used for imaging from the air side of the film. In both geometries the sample, together with the excitation source, is scanned using a piezo-electrically driven stage while the collection optics is kept fixed. The collected luminescence is guided through a fiber to a spectrograph and a Si CCD detector, to spectrally separate the different Er upconversion luminescence lines. The spectra are integrated from 510 to 570 nm and from 640 to 700 nm to obtain images of the upconversion luminescence from the $^4S_{3/2}/^2H_{11/2}$ and $^4F_{9/2}$ Er^{3+} levels, respectively.

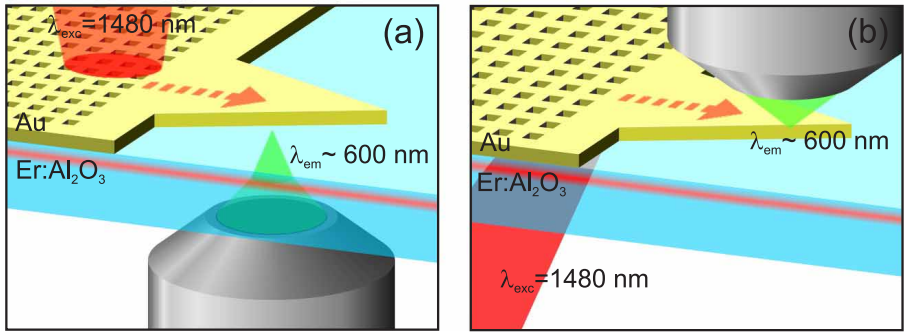

Fig. 2. Schematic of the experimental geometry in the case of upconversion luminescence detection through the substrate (a), or from the air side of the sample (b). In both cases the SPPs are excited with infrared light at the Au/Al_2O_3 interface in the direction of the arrow. The red line schematically indicates the Er depth profile.

3. Results and discussion

Figure 3(a) shows a two-dimensional image of the 550 nm upconversion luminescence intensity, obtained as described above with an excitation power of 20 mW at 1.48 µm. The luminescence is collected through the substrate, i.e., from the side of the Au film where the SPPs are excited and the Er ions are located. In the left of the image, indicated by the arrow, the excitation spot on the hole array can be recognized. An excited SPP beam is visible that exits the excitation array to the right and is coupled into the tapered waveguide, which starts at x = 16 µm. Along the taper an interference pattern is observed and the upconversion luminescence intensity gradually increases as the beam propagates further into the taper. The interference pattern can be ascribed to the reflection of the infrared SPP beam at the sides of the tapered waveguide [2,19], which causes the optical energy to be concentrated as the waveguide width keeps decreasing. From x = 60 µm onwards toward the apex, only a single maximum is observed across the waveguide.

#89786 - $15.00 USD Received 14 Nov 2007; revised 19 Dec 2007; accepted 19 Dec 2007; published 2 Jan 2008

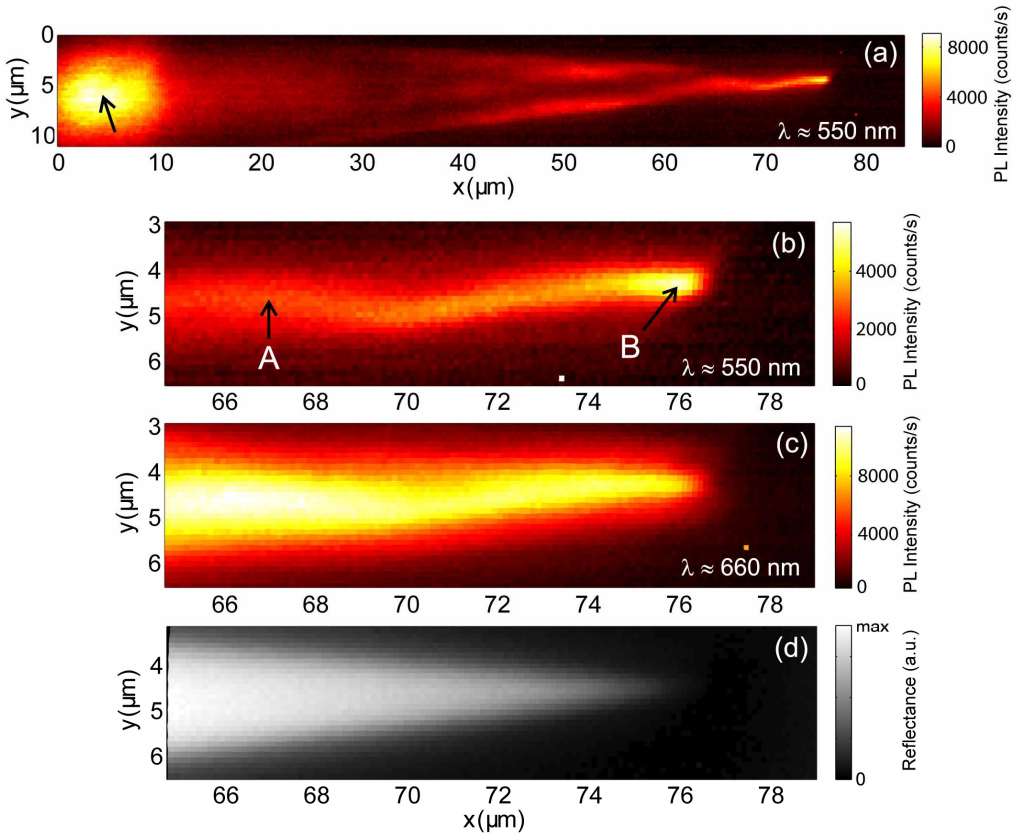

Fig. 3. (a) Upconversion luminescence image from the hole array (left side) and 60 μm long tapered waveguide (right side) sections, taken at 550 nm. The excitation spot is marked by the arrow on the left side of the image. (b) and (c): Detailed maps of the upconversion intensity near the tip of the waveguide, taken at 550 nm and 660 nm, respectively. A 1.48 μm pump at a power of 20 mW was used. The arrows indicate the positions at which power dependency curves were obtained. (d) Optical microscopy image of the same region as (b) and (c), obtained by detecting reflected light from a halogen lamp at a wavelength of 550 nm.

Shown in Figs. 3(b) and 3(c) are images of the last 12 μm of the taper, obtained by detecting luminescence from the 550 nm and 660 nm Er levels, respectively. To indicate the position of the taper tip in these figures, Fig. 3(d) shows an image of the same scan area obtained by collecting normal-incident reflected light at a wavelength of 550 nm. A clear difference is noticeable between the images of the luminescence taken with 550 and 660 nm detection wavelengths. Whereas the intensity of the 660 nm upconversion luminescence is rather constant along the last 12 μm of the tapered waveguide, the 550 nm luminescence intensity shows a marked increase towards the tip. The spot of maximum intensity is achieved within the last 2 μm of the taper, where the lateral width of the waveguide is less than 400 nm. The 550 nm luminescence intensity in this spot is more than 10 times larger than at the start of the tapered waveguide. The differences between Figs. 3(b) and (c) can be explained through the different pump power dependencies of the nonlinear excitation of these two Er levels. While three infrared pump photons are needed to excite one ion to the $^4F_{9/2}$ state emitting at 660 nm, four are needed to populate the $^4S_{3/2}$ manifold emitting at 550 nm. The emission at 550 nm therefore exhibits a stronger dependence on the local SPP field intensity than the 660 nm luminescence.

Given this argument, it may seem surprising that the intensity of the 550 nm luminescence collected at x = 76 μm (position B) is two times higher than that at x = 67 μm (position A), while the 660 nm luminescence at position B is actually slightly smaller than at position A. We attribute this to an effect related to the spatial resolution of the detection,

#89786 - $15.00 USD Received 14 Nov 2007; revised 19 Dec 2007; accepted 19 Dec 2007; published 2 Jan 2008

which is ~800 nm. Suppose that the SPP field is concentrated at position B to a spot smaller than the focal area, and less so at position A. In that case, it is possible that the averaged 660 nm upconversion luminescence intensity in the focal area is equal at both positions, while the averaged 550 nm intensity at position B is larger than that in A, as this level is populated by a higher-order nonlinear process.

The previous considerations suggest the importance of investigating the power dependence of the upconversion luminescence intensity at different positions along the waveguide. Figure 4 shows the upconversion luminescence at 550 nm and 660 nm measured at positions A and B indicated in Fig. 3(b), as a function of the excitation laser power. The local pump intensity that is responsible for the generation of upconversion luminescence scales linearly with the excitation laser power, and it can be different at both positions for a particular excitation power. The data is plotted on a double-logarithmic scale. The numbers in the figure indicate the slopes of linear fits to the logarithm of the data with luminescence intensity between 100 and 1000 counts/s. We first note that the slopes of the power dependence curves in Fig. 4 differ from the values expected in the limit of infinitely small pump power. These are 3 and 4 for the levels emitting at 660 nm and 550 nm, respectively. Even at moderate SPP excitation intensities, saturation of the various Er levels can reduce the slope significantly [25,27]. If we assume 100% coupling efficiency of the incident light to SPPs propagating out of the excitation array, we can estimate an upper limit of the local SPP intensity just outside the array at the depth of the Er ions to be 0.6 MW/cm^2 for the 20 mW incident power. For such excitation power densities and the Er concentration used here, large saturation effects are indeed expected [25]. Comparing the slopes at different positions, it is found that for both detection wavelengths the slope at position B is significantly less than the slope at position A. This implies that at the tip of the waveguide (position B) the Er energy levels are more strongly saturated. Hence the SPP field intensity in that position is larger. At relatively low excitation laser powers, we can see from Fig. 4 that the detected upconversion intensity at the tip exceeds that at position A also for the 660 nm luminescence, since the effect of saturation is smaller in that regime.

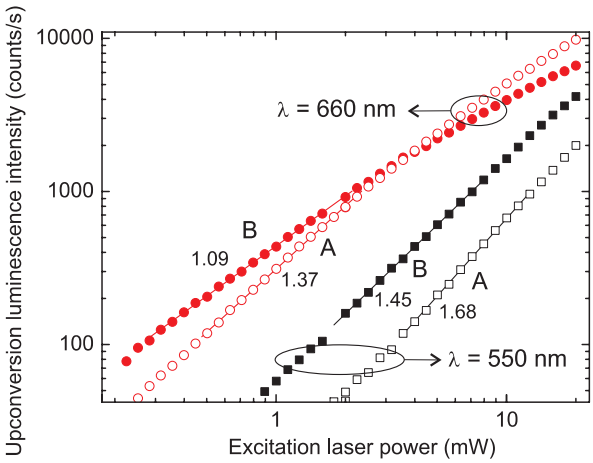

Fig. 4. Excitation laser power dependence ($\lambda = 1.48$ μm) of the upconversion luminescence at 550 and 660 nm collected at positions A and B (indicated with arrows in Fig. 3(b)). The lines are linear fits to the data for luminescence intensities between 100 and 1000 counts/s, and the slopes of these fits are indicated. The error in the fit is of order 0.01.

Even when considering pump conditions at positions A and B that result in an equal detected upconversion luminescence intensity (see Fig. 4), the difference in the slope of the curves at these excitation laser powers indicates that there is a clearly different amount of saturation at both positions. This observation strongly suggests that the local excitation field is indeed not homogeneously distributed within the focal area: at the tip (position B) the excitation field is

#89786 - $15.00 USD Received 14 Nov 2007; revised 19 Dec 2007; accepted 19 Dec 2007; published 2 Jan 2008

concentrated to dimensions smaller than the microscope resolution. When averaging the upconversion luminescence over the focal area, this results in approximately equal detected intensities for the 660 nm luminescence in Fig. 3(c), even though the *maximum* SPP intensity at the tip is actually larger than the intensity at position A. This SPP concentration is revealed through the observed increase in saturation at the tip. As mentioned before, the level emitting at 550 nm is populated through a higher-order nonlinear process, so the increased SPP intensity at the tip (position B) with respect to position A can be apparent from both the enhanced upconversion intensity and the increased saturation at the tip. Still, for both wavelengths focal averaging limits the detection of the maximum luminescence intensity at the tip. With these considerations, both the observed difference between the intensity maps taken at different wavelengths as well as the behavior of the pump power dependencies at positions A and B can be explained in terms of an enhanced SPP field at the tip.

We note that towards the taper end, the radiative decay rate of the Er energy levels could change as a result of a change in the local optical density of states. The observed enhanced upconversion near the tip could be ascribed to an enhanced radiative decay rate; however, this is inconsistent with the larger degree of saturation near the tip. Although an effect of the taper on the emission rates cannot be excluded, it cannot be the dominant mechanism behind the observed luminescence enhancement near the tip.

The broad lateral intensity variations along the length of the taper in Fig. 3(a) are explained by interference due to reflection of SPP waves at the metal taper edge [2,19]. In addition to this effect, we conclude from these experiments that the SPP fields are further concentrated along the last stretch of the tapered waveguide, to the position of maximum intensity observed in Fig. 3(b). The precise determination of the location of maximum SPP intensity with respect to the taper apex is limited by the spatial resolution of the microscope. To investigate this further, Fig. 5 shows upconversion luminescence images collected from the air side of the film for 550 nm and 660 nm (see Fig. 2(b) for experimental configuration). In this case, the SPPs on the metal-substrate interface are excited by illuminating the hole array through the substrate under a properly chosen angle. This geometry allows the use of an objective with a larger numerical aperture for collecting the luminescence, which results in a higher spatial resolution compared to Fig. 3. The position of the edge of the taper derived from electron microscopy data is drawn as a dotted line. Although the sample is now imaged from the side of the Au film opposite to the Er-doped substrate, clear Er upconversion luminescence is detected both through the holes and at the edges of the waveguide. A maximum is observed at the taper tip for both wavelengths. The detected 550 nm luminescence intensity at the tip is much larger than the intensity along the edges of the rest of the waveguide. The luminescence at the edges is hard to discern in the 550 nm luminescence intensity image as the color scale is scaled to the intensity at the tip. As in the previous experimental geometry, the luminescence increase at the tip is stronger for 550 nm luminescence than for the 660 nm luminescence. Although the role of diffraction of the luminescence at the metal edges makes a quantitative interpretation of these images difficult, we note that the maxima are observed at a distance less than 1.0 μm from the tip, corresponding to a waveguide width smaller than 200 nm.

In the experiments presented in Figs. 3 and 5 no indication is found that the mode propagating along the tapered waveguide experiences cutoff for a particular waveguide width. Such a cutoff width was predicted to exist for the SPP modes supported by a stripe waveguide on a dielectric substrate, both the leaky modes at the air side of the metal film and the bound modes at the substrate side [28]. In that work, a cutoff stripe width of ~500 nm was calculated for the bound mode for a free-space wavelength of 800 nm. The cutoff results from a decreased wave vector, and hence reduced mode confinement in narrower waveguides. As a result, this mode could not exhibit focusing along a tapered waveguide. The fact that in the experiment reported here no cutoff behavior is observed down to a width smaller than 400 nm, for a wavelength much larger than that used in reference [28], suggests that another mode may be involved in the focusing that does not experience cutoff and that becomes more strongly confined to the waveguide as the width decreases.

#89786 - $15.00 USD Received 14 Nov 2007; revised 19 Dec 2007; accepted 19 Dec 2007; published 2 Jan 2008

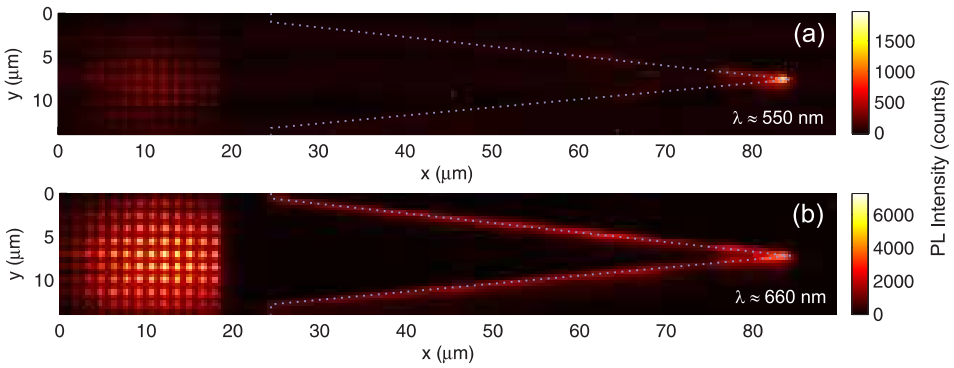

Fig. 5. Upconversion luminescence images taken from the air side of the film at (a) 550 nm and (b) 660 nm. The edge of the taper is indicated by the dotted line. Upconversion luminescence excited by SPPs on the substrate side of the film is observed from the edges of the taper, and the maximum intensity is detected at the taper tip.

4. Modeling

To investigate the absence of cutoff and the observed concentration up to very narrow waveguide widths we perform three-dimensional simulations of the electromagnetic fields in the tapered waveguide structure. A finite-difference time-domain (FDTD) algorithm [29] is used to calculate the time-averaged field intensity in the structure upon excitation of a SPP mode at the substrate side of the film. Additionally, a comparison is made with excitation of the SPP mode at the low-index side of the waveguide. Modes localized at different sides of a metal film embedded in an asymmetric dielectric environment generally have different properties, as sketched in Fig. 6(a) [9,28,30]. On a metal film of infinite lateral extension, the SPP mode that has most of its field energy localized in the high-index substrate is called asymmetric since its transverse electric field has an opposing sign at either side of the metal film. The sign of the surface charge at both metal/dielectric interfaces is equal for this mode. In contrast, the mode propagating predominantly at the low-index side of the film has electric fields with equal sign at both sides of the film, and is therefore called symmetric. Accordingly, the surface charge at both interfaces associated with this mode has an opposite sign.

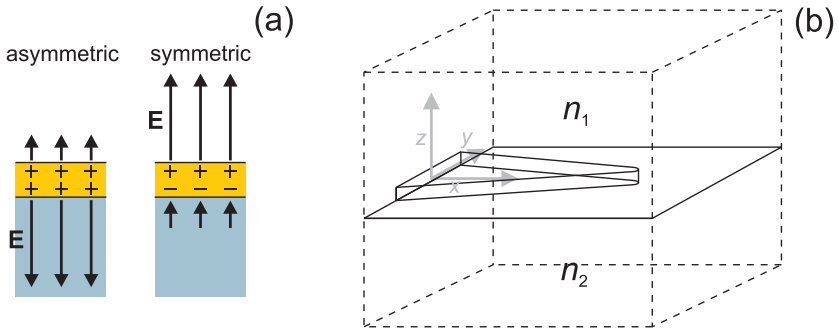

Fig. 6. (a) Sketch of the electric field of the two SPP modes in an infinitely extended metal film, showing the symmetry of the transverse electric field and the surface charge. The direction of propagation is normal to the image plane. (b) Schematic of the geometry used in the FDTD calculations. The Au taper has a length of 7.8 μm and an apex diameter of 60 nm. The refractive index of the substrate is n_2, and that of the surrounding medium is n_1.

The simulation geometry is displayed schematically in Fig. 6(b). All structural parameters are taken the same as in the experiment. The tip of the taper is rounded in the *x*,*y* plane with an apex diameter of 60 nm, consistent with the experimentally investigated apex. Only

#89786 - $15.00 USD Received 14 Nov 2007; revised 19 Dec 2007; accepted 19 Dec 2007; published 2 Jan 2008

propagation on the last 7.8 µm of the tapered waveguide is calculated to reduce the computational effort. This does not allow resolving the large scale interference pattern caused by reflection at the waveguide edges that was observed in Fig. 3(a), but it provides insight in the behavior of SPPs in the region of interest, corresponding to Figs. 3(b-c). Perfectly matched layer simulation boundaries are used around the structure to absorb all radiated power as well as SPPs reflected in the negative x direction. Electric field symmetry is assumed with respect to the $y = 0$ plane. The Au permittivity is modeled by a Drude model including damping, of which the parameters are obtained by fitting the optical constants given by Johnson and Christy [31] around a wavelength of 1.48 µm. The discretization step inside the metal is varied from 4.5 nm at the start of the taper to 3 nm in the vicinity of the apex. The excitation source is a 25 fs pulse with a center frequency corresponding to a free-space wavelength of 1.48 µm. It is injected in the positive x direction at $x = 0$ and has a transverse (yz) field profile identical to a SPP mode profile of a waveguide with a width of 1.56 µm. This SPP mode profile is calculated by a finite-difference frequency domain mode solver, described in reference [32], which uses the same spatial discretization as the FDTD simulation. Steady-state time-averaged field intensity profiles corresponding to a free-space wavelength of 1.48 µm are obtained by Fourier transforming the fields obtained from the FDTD simulation.

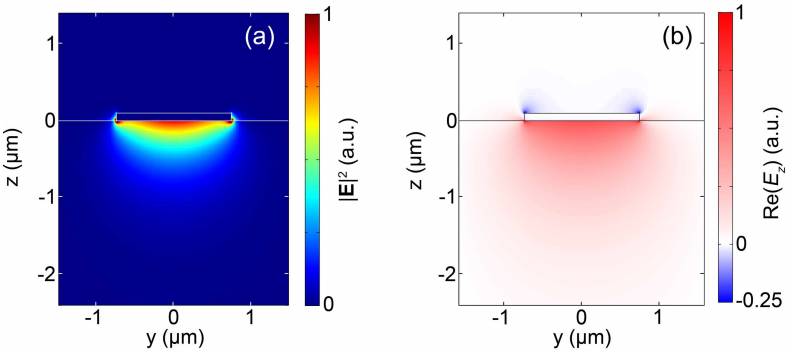

Fig. 7. Mode profile of the asymmetric bound mode used as excitation source at $x = 0$ in the FDTD simulation. Shown are the electric field intensity (a) and the real part of the electric field component in the z direction (b).

Figure 7(a) shows the electric field intensity profile of the purely bound SPP mode that is excited at the start of the tapered waveguide. The strongest component of the electric field is directed normal to the film (E_z) [30]; its real part is plotted in Fig. 7(b). From the opposing signs of E_z at both sides of the metal film it can be seen that the transverse electric field is asymmetric across the film. As mentioned before, this is characteristic for a mode localized at the substrate side of the film [9,30]. The calculated mode profile does not possess any field nodes along the width of the structure, and thus the induced surface charge has equal sign along the complete circumference of the waveguide. Although the mode possesses strong fields at the metal corners [30], a large fraction of its energy is contained in a single broad intensity maximum under the waveguide. It is therefore likely to be efficiently excited in our experiment.

The result of the FDTD simulation using the profile of Fig. 7(a) as input is shown in Fig. 8. Figure 8(a) shows the time-averaged electric field intensity in the plane $z = -35$ nm, which is the depth at which the Er ions are located in the experiment. Three observations can be made. First, the field is strongly concentrated at the taper tip, to a spot much smaller than the wavelength of light in the substrate. The full width at half maximum of this spot in the y direction is 92 nm, which is limited by the 60 nm apex diameter. Second, no sign of a cutoff width is observed. Third, a pronounced interference pattern can be seen that extends to the end of the taper and has a periodicity of half the SPP wavelength. This suggests that the SPP wave propagating in the taper is reflected from the extremity of the tip. It resembles observations on

#89786 - $15.00 USD Received 14 Nov 2007; revised 19 Dec 2007; accepted 19 Dec 2007; published 2 Jan 2008

SPPs propagating along a thin metal nanowire, which also show strong reflections from the nanowire ends [33].

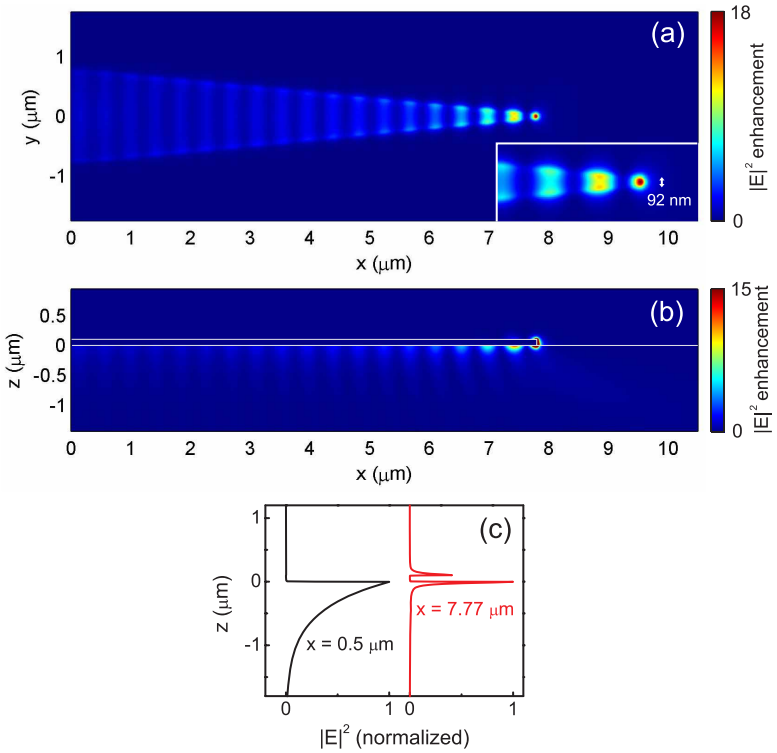

Fig. 8. Electric field intensity in the planes z = -35 nm (a), and y = 0 (b). The scale is normalized to the average intensity at the start of the tapered waveguide. Both color scales are saturated to improve the visibility away from the tip. The intensity enhancement at z = -10 nm below the tip apex is 100. The inset of (a) shows a detail of the electric field intensity in the plane z = -35 nm at the tip. The intensity distribution at the tip has a full width at half maximum of 92 nm. Normalized vertical cross sections of (b) at the start (x = 0.5 μm, black) and the end (x = 7.77 μm, red) of the taper are depicted in (c), showing the increase of vertical confinement towards the taper tip.

Figure 8(b) shows a cross cut of the electric field intensity $|\mathbf{E}|^2$ in the structure along the y = 0 plane. At the tip at a depth of 10 nm below the film, the electric field intensity is enhanced by more than a factor 100 with respect to the start of the tapered waveguide (not visible in the scale bar due to saturation in the color scale). This enhancement is limited by the finite sharpness of the tip. Figure 8(b) also shows that the SPP field becomes much more confined in the transverse (z) direction as the taper tip is approached. In Fig. 8(c) the electric field intensity is plotted as a function of z for the start and the end of the taper. At the end of the taper the SPP intensity decays in a few tens of nm from the metal/substrate interface; more than an order of magnitude faster than at the start. Clearly, the field is truly concentrated to nanoscale transverse dimensions, remaining tightly confined to the metal surface. Figure 8(c) also shows that for very narrow widths a significant intensity builds up at the air side of the metal film. This is further illustrated in Fig. 9, which shows a cross-section of the field intensity at the taper tip in the plane x = 7.77 μm, where the Au taper width is only 60 nm. The field is predominantly localized at the metal corners, but no nodes are observed in the field around the tapered waveguide. This indicates that also in this plane the surface charge has identical sign around the waveguide, and that the transverse electric field across the waveguide must thus be asymmetric. This symmetry strongly resembles that of the azimuthally symmetric mode supported by a metal cylinder embedded in a homogeneous dielectric background, which is predicted to allow nanofocusing in a conical waveguide [11].

#89786 - $15.00 USD Received 14 Nov 2007; revised 19 Dec 2007; accepted 19 Dec 2007; published 2 Jan 2008

Our results therefore show that similar nanofocusing is possible in all-planar geometries provided that the proper mode is excited.

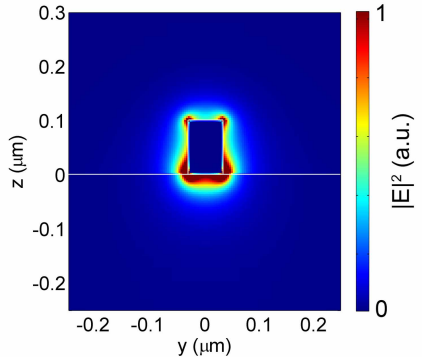

Fig. 9. Cross section of the electric field intensity near the tip of the tapered waveguide, at $x = 7.77$ μm. The field is predominantly localized at the metal corners. No field nodes are present along the metal surface.

Finally, we investigate if nanoscale focusing in planar waveguide tapers could also be possible when leaky symmetric SPP modes localized at the low-index side of the film are excited, and compare it to the behavior of bound SPPs at the high-index side of the film. This is relevant since SPPs at the low-index side of the film have been extensively studied in stripe waveguides, because they can be probed at high resolution using near-field microscopy [2,5,21]. To make a fair comparison, the effective guiding index of the two types of modes should be as close as possible in order not to affect cutoff conditions solely because of a difference in SPP wave vector. To study symmetric modes we therefore consider a structure in which the refractive index above the metal film is $n_1 = 1.74$ (equal to that at the substrate for the asymmetric mode calculations). The refractive index of the substrate is increased such that the ratio n_1/n_2 is the same as before ($n_2 = 1.74^2$). Because the mode solver we used does not solve for leaky modes, we now use an array of ten coherent oscillating dipoles oriented along the z direction as excitation source in the FDTD calculation. The dipoles are positioned at a line parallel to the y direction, at a distance of 10 nm from the film, either in the high-index material to excite asymmetric modes (at $x = 0$, $z = -10$ nm) or in the low-index material to excite symmetric modes ($x = 0$, $z = 110$ nm). Figure 10 shows the electric field intensity in the plane $y = 0$ for both cases. Figure 10(a) shows the result for dipole excitation at the high-index side of the film; as expected, the result is very similar to that in Fig. 8(b), indicating that a mode is excited with the ability to cause nanofocusing. Figure 10(b) shows the result for excitation at the low-index side of the film. Now the behavior is completely different. Surface-bound waves are observed, but no concentration effect is visible at the taper tip. No reflection of SPPs from the tip is observed. This behavior is in agreement with earlier work that predicted that as the waveguide width is decreased, the mode effective index of the symmetric leaky mode will decrease and transverse confinement will be reduced [28]. As the mode gets less confined in the y direction, more energy is lost to radiation into the high-index dielectric substrate, and losses will increase. After a certain cutoff width, only radiation modes contribute to the local field [21], which cannot cause focusing to nanoscale dimensions.

As can be seen from these simulations, the excitation of a SPP mode that is guided and concentrated to arbitrarily small widths is only possible with the asymmetric bound mode of the stripe waveguide, and hardly with a symmetric leaky mode. This is due to the fact that only the former possesses the correct symmetry to cause nanofocusing. The fact that the predicted intensity enhancement and standing wave pattern are not fully reproduced in the detected upconversion luminescence is attributed to a combination of focal averaging and

#89786 - $15.00 USD Received 14 Nov 2007; revised 19 Dec 2007; accepted 19 Dec 2007; published 2 Jan 2008

saturation of the excited Er levels, possibly in conjunction with losses due to surface and sidewall roughness [33]. We conclude that nanoscale focusing can be obtained at the taper tip to dimensions and intensities that are only limited by the sharpness of the taper apex.

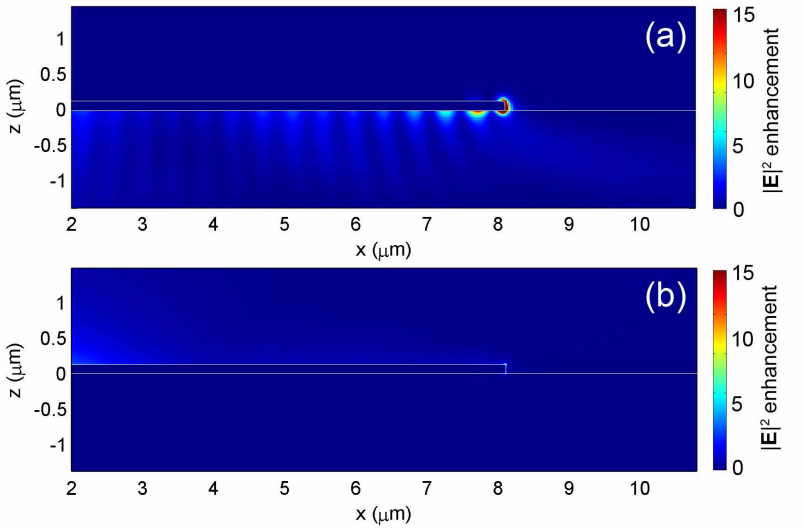

Fig. 10. Electric field intensity in the $y = 0$ plane for the asymmetric bound mode at the high index side of the film (a), and the symmetric leaky mode at the low index side of the film (b). The color scale is saturated in (a), and the same for both figures.

5. Conclusions

We have shown experimentally that guiding and focusing of surface plasmon polaritons (SPPs) is possible in laterally tapered Au waveguides on a planar dielectric substrate when the proper initial SPP mode is excited. For the asymmetric bound mode propagating at the substrate side of the film with 1.48 μm light, experiments show concentration occurring beyond a waveguide width smaller than 400 nm. No sign of a cutoff width is observed along the taper. By comparing the spatially-resolved upconversion intensities and power dependencies of emission from different Er levels, we conclude that SPP focusing is the dominant mechanism producing the spot of maximum intensity at the taper tip. FDTD simulations corroborate these results and show that focusing down to truly nanoscale volumes is possible in this geometry. The nanofocusing is attributed to a guided SPP mode that has an asymmetric electric field distribution across the tapered waveguide. For symmetry reasons, efficient nanofocusing cannot be achieved with symmetric leaky SPP modes propagating at the low-index side of the film. Varying parameters such as film thickness, tapering angle, excitation frequency and tip sharpness is expected to allow optimization of the possible field enhancements and focusing efficiency. A geometry such as this could serve as a useful interface between micro- and nano-scale optics.

Acknowledgements

The authors would like to thank C. Rétif and N. de Jong for the development of fabrication procedures using a negative resist. This work was made possible by the fabrication and characterization facilities of the Amsterdam nanoCenter. It is part of the Joint Solar Programme (JSP) of the Stichting voor Fundamenteel Onderzoek der Materie (FOM), which is financially supported by the Nederlandse organisatie voor Wetenschappelijk Onderzoek (NWO). The JSP is co-financed by gebied Chemische Wetenschappen of NWO and Stichting Shell Research.

#89786 - $15.00 USD Received 14 Nov 2007; revised 19 Dec 2007; accepted 19 Dec 2007; published 2 Jan 2008